Heisenberg spin triangles in $\{V_6\}$-type magnetic molecules: Experiment and theory

Marshall Luban,[1,*] Ferdinando Borsa,[1] Sergey Bud'ko,[1] Paul Canfield,[1] Suckjoon Jun,[2] Jae Kap Jung,[3] Paul Kögerler,[1] Detlef Mentrup,[4] Achim Müller,[5] Robert Modler,[1] Daniel Procissi,[1] Byoung Jin Suh,[6] and Milton Torikachvili[7]

[1]*Ames Laboratory and Department of Physics and Astronomy, Iowa State University, Ames, Iowa 50011*

[2]*Department of Physics, Simon Fraser University, Burnaby, BC, Canada V5A 1S6*

[3]*Division of Electromagnetic Metrology, Korea Research Institute of Standards and Science, Daejeon, 305-600, Korea*

[4]*Fachbereich Physik, Universität Osnabrück, D-49069 Osnabrück, Germany*

[5]*Anorganische Chemie I, Universität Bielefeld, D-33501 Bielefeld, Germany*

[6]*Department of Physics, The Catholic University of Korea, Puchon, 420-743, Korea*

[7]*Department of Physics, San Diego State University, San Diego, California 92182*

(Received 19 February 2002; published 5 August 2002)

We report the results of systematic experimental and theoretical studies of two closely related species of magnetic molecules of the type $\{V_6\}$, where each molecule includes a pair of triangles of exchange-coupled vanadyl (VO^{2+}, spin $s=1/2$) ions. The experimental studies include the temperature dependence of the low-field susceptibility from room temperature down to 2 K, the dependence of the magnetization on magnetic field up to 60 T for several low temperatures, the temperature dependence of the magnetic contribution to the specific heat, and the ^{1}H and ^{23}Na nuclear magnetic resonance spin-lattice relaxation rates $1/T_1$. This body of experimental data is accurately reproduced for both compounds by a Heisenberg model for two identical uncoupled triangles of spins; in each triangle, the spins interact via isotropic antiferromagnetic exchange, where two of the three V-V interactions have exchange constants that are equal and an order of magnitude larger than the third; the ground-state eigenfunction has total spin quantum number $S=1/2$ for magnetic fields below a predicted critical field $H_c \approx 74$ T and $S=3/2$ for fields above H_c.

DOI: 10.1103/PhysRevB.66.054407 PACS number(s): 75.10.Jm, 75.50.Xx, 76.60.−k, 36.40.Cg

I. INTRODUCTION

The subject of magnetic molecules has greatly advanced in recent years due to notable progress[1–4] in synthesizing bulk samples of identical molecular-size units each containing a relatively small number of paramagnetic ions (''spins'') that mutually interact via Heisenberg exchange. In the great majority of cases the intermolecular magnetic interactions (typically dipole-dipole in origin) are negligible as compared to the intramolecular exchange interactions. Measurements of the magnetic properties therefore usually reflect those of a common, individual molecular unit. At one extreme one has the largest magnetic molecule synthesized to date, the giant Keplerate species $\{Mo_{72}Fe_{30}\}$ with 30 interacting Fe^{III} ions (spins with $s=5/2$) forming a highly symmetric array incorporated in the diamagnetic framework of a synthetic host molecule with diameter 2.5 nm.[5] This number of interacting high-spin ions is far larger than what might ever be dealt with by a complete matrix-diagonalization procedure. It is therefore of great interest to also thoroughly investigate magnetic molecules at the other extreme: namely, where the number of interacting spins is so small that exact statistical mechanical calculations can be performed and the emerging results can be directly compared to the results of experiment. This is the situation for both species of magnetic molecules[6] studied in the present work, where we provide strong evidence supporting the picture that each molecule can be described in terms of two identical uncoupled triangular units. A triangular unit is formed by three exchange-coupled spins (VO^{2+} ions,[7] $s=1/2$). These species thus provide realizable examples of an idealized or ''textbook'' model system, where the energy eigenvalues and eigenvectors and all thermodynamic quantities can be calculated in closed form. This unusual opportunity for providing a comprehensive analytical treatment of an interacting Heisenberg spin system has motivated us to provide an equally comprehensive experimental study. The primary goals are, first, to establish the salient magnetic properties of these interacting spin systems and, second, to develop a consistent theoretical description based on the Heisenberg model that is in very good agreement with the variety of experiments we have performed.

We are concerned with two species of polyoxovanadate-based magnetic molecules, labeled **1** and **2**, with the chemical formulas $(CN_3H_6)_4Na_2[H_4V_6^{IV}O_8(PO_4)_4\{(OCH_2)_3CCH_2OH\}_2]\cdot 14H_2O$ (**1**) and $Na_6[H_4V_6^{IV}O_8(PO_4)_4\{(OCH_2)_3CCH_2OH\}_2]\cdot 18H_2O$ (**2**). The structures of these species are illustrated in Figs. 1(a) and 1(b). Single-crystal x-ray analysis has established[6] that in **1** the distances between the three V^{IV} ions are 3.218 (V1-V2), 3.222 (V1-V3), and 3.364 (V2-V3) Å. In **2** the corresponding distances are 3.212, 3.253, and 3.322 Å. This initially led us to anticipate that two, nearly equal exchange constants would be necessary and sufficient for defining the Heisenberg model Hamiltonian for each interacting three-spin triangle. However, although the V···V distances are nearly equal, of greater importance is the fact that only two of the three pairs of ions are linked by strong[8] O-P-O exchange pathways [see Fig. 1(b) and the Appendix]. Hence it is not unreasonable that the exchange constants may differ greatly. In the following we denote the two exchange constants by J_a, for the two nearly equal bonds, and J_c, for the remaining bond.

The layout of this article is as follows: In Sec. II we derive the thermodynamic properties (magnetic equation of state and specific heat) of a Heisenberg spin triangle and

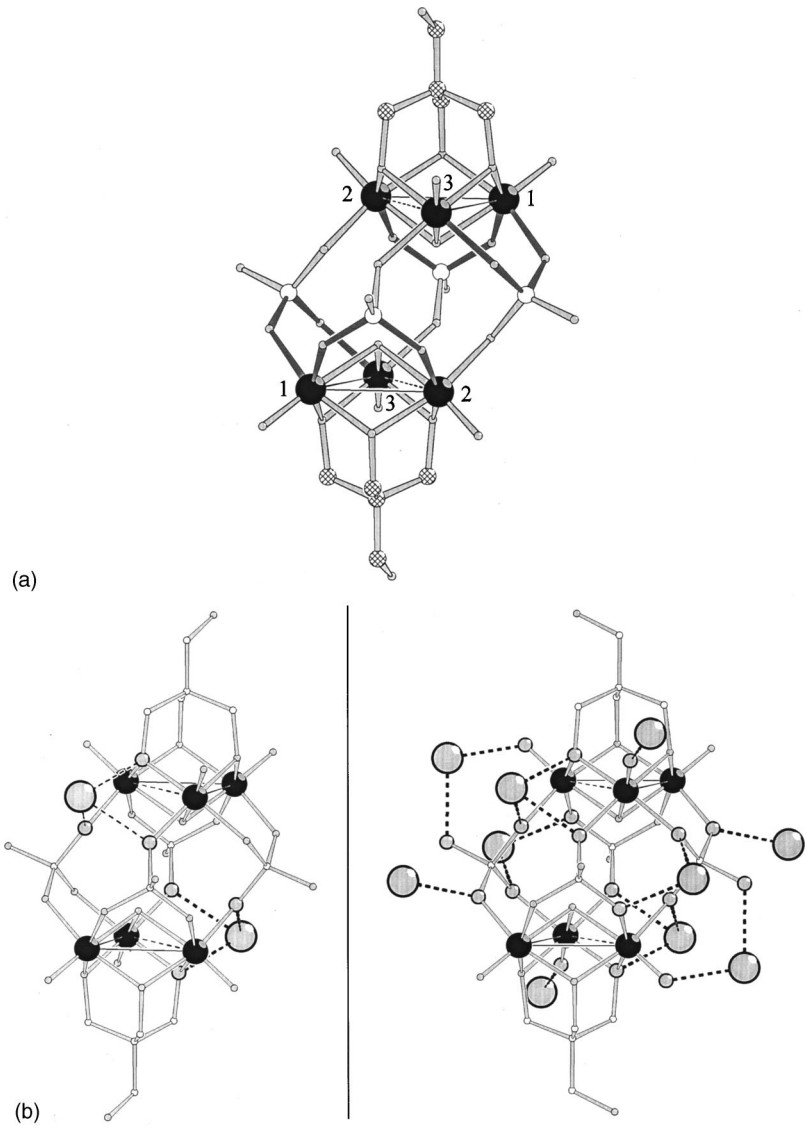

FIG. 1. (a) Ball-and-stick representation of the $\{V_6\}$ cluster anion with numbering of the V^{IV} centers (V: large black spheres; P: white spheres; C: white cross-hatched spheres; O: small gray spheres; H positions not shown). The V-O-P-O-V superexchange pathways linking the pairs of ions 1,2 and 1,3 are emphasized as dark gray bonds. The absence of such a pathway for the pair 2,3 is the primary factor responsible for the great disparity in the numerical values of the exchange energies $J_{12}=J_{13}\equiv J_a$ (solid line), $J_{23}\equiv J_c$ (dashed line). (b) Representation of the closest contacts ($Na\cdots O=2.3-2.6$ Å, thick dashed lines) between sodium cations and oxygen centers belonging to the $\{V_6\}$ anion in the crystal lattices of **1** (left) and **2** (right). Sodium cations are shown as large gray outlined spheres; the oxygen positions closest to the Na^+ positions are also shown enlarged and outlined.

compare with our experimental data for the two species of $\{V_6\}$-type magnetic molecules. In particular, we derive the energy levels of the Heisenberg model for three spins $s=1/2$ with distinct exchange constants in Sec. II A and the expression for the partition function in Sec. II C. As explained in Sec. II B, it turns out that three distinct exchange constants, one for each pair of spins, are superfluous. One can only determine two of the exchange constants by thermodynamic measurements, because of a special property of the general Heisenberg system of three interacting $s=1/2$ spins, referred to as isospectrality.[9] We also provide an expression [see Eq. (4) below] for the thermal equilibrium magnetic moment $M(T,H)$ of this system and outline its major properties. In Sec. II C 1 we give our experimental results for the temperature dependence of the low-field magnetic susceptibility from room temperature down to 2 K for both compounds. Comparing these data with the theoretical susceptibility, we establish the values of the exchange constants J_a and J_c for each compound. In Sec. II C 2 we also give our experimental results for the field dependence of $M(T,H)$ up to 60 T for several temperatures below 20 K. In Sec. II C3 we give the temperature dependence of the specific heat difference $C(T,H)-C(T,0)$ for $T<12$ K and $H=9$ T. In Sec. III A we present our results for the temperature and field dependence of the spin-lattice relaxation rate $1/T_1$ as obtained by both ^{1}H and ^{23}Na nuclear magnetic resonance (NMR) methods. In Sec. III B we compare with theoretical results using the standard Moriya formula[10] for $1/T_1$. That formula relates the spin-lattice relaxation rate to the thermal equilibrium time correlation functions of the exchange-coupled paramagnetic ions, quantities which we have calculated for the Heisenberg triangle. Comparison between theory and experiment can thus provide[11] an effective technique for determining the low-frequency characteristics of the dynamics of the paramagnetic ions in magnetic molecules.

All of these diverse experimental data, given in Secs. II and III, are in good agreement with our theoretical predictions based on the Heisenberg model using the values of the two exchange constants as inferred from the measured temperature dependence of the low-field susceptibility. A summary and discussion is presented in Sec. IV. Finally, in the

Appendix we summarize the most important aspects of the chemical structure of the two compounds studied here.

II. MAGNETIZATION AND SPECIFIC HEAT

A. Theoretical model

The model we adopt for describing the magnetic molecules **1** and **2** is that of two identical, but magnetically independent triangular arrays of three spins $s=1/2$. The three spins are chosen to interact with one another via isotropic exchange as well as with a uniform static external magnetic field H according to the Hamiltonian

$$\mathcal{H}=J_a(\mathbf{S}_1\cdot\mathbf{S}_2+\mathbf{S}_1\cdot\mathbf{S}_3)+J_c\mathbf{S}_2\cdot\mathbf{S}_3+\mu H(S_{1z}+S_{2z}+S_{3z}). \tag{1}$$

The exchange constants J_a and J_c are positive energies corresponding to antiferromagnetic coupling, $\mu=g\mu_B$, g is the spectroscopic splitting factor, μ_B denotes the Bohr magneton, the direction of the external magnetic field defines the z direction, and the spin operators are given in units of $\hbar$. The numerical values of the three parameters J_a, J_c, and g are determined in Sec. II C 1 by comparing the predictions based on Eq. (1) with our experimental data for the magnetic susceptibility. As discussed in the Appendix the chemical structure of **1** and **2** is such that the exchange interaction between spins 1 and 2 should very nearly equal that between spins 1 and 3, which in turn are distinct from the exchange interaction between spins 2 and 3. We shall refer to Eq. (1) as the Hamiltonian for an ''isosceles Heisenberg triangle'' of spin 1/2.

The eigenvalues of H given in Eq. (1) can easily be derived by simple algebraic methods. Introducing the total spin operator $\mathbf{S}=\mathbf{S}_1+\mathbf{S}_2+\mathbf{S}_3$, the pair spin operator $\mathbf{S}_{23}=\mathbf{S}_2+\mathbf{S}_3$, as well as the constants $J=(2J_a+J_c)/3$ and $\Delta=J_a-J_c$, one can rewrite $\mathcal{H}$ as

$$\mathcal{H}=\left(-\frac{9}{8}J+\frac{3}{8}\Delta\right)+\frac{1}{2}\left(J+\frac{\Delta}{3}\right)S^2-\frac{1}{2}\Delta S_{23}^2+\mu HS_z. \tag{2}$$

Now S^2, S_z, S_{23}^2, and $\mathcal{H}$ mutually commute, and thus the eigenvectors of $\mathcal{H}$, denoted by $|S,M_S,S_{23}\rangle$, are simultaneous eigenvectors of the first three operators. The explicit forms of the energy eigenvectors in terms of the spin-up and spin-down states of the individual spin operators are given elsewhere.[12] In the field-free case there are three distinct energy levels. The ground state and first excited levels are each doubly degenerate ($S=1/2$), and they are separated by an energy gap which equals $|\Delta|$. Besides $S=1/2$, the ground-state level is also characterized by the quantum number $S_{23}=1(0)$ if $\Delta>(<)0$, respectively. The second excited level is fourfold degenerate ($S=3/2$), and its energy is $(3J+|\Delta|)/2$, as measured from the ground-state level. A schematic diagram of the energy levels including the effects of the magnetic field is given in Fig. 2. For the special case $\Delta=J_a-J_c=0$ (equilateral case) the ground-state eigenvector for $H=0$ is fourfold degenerate, whereas these four levels are split into two doubly degenerate levels for $H\neq 0$.

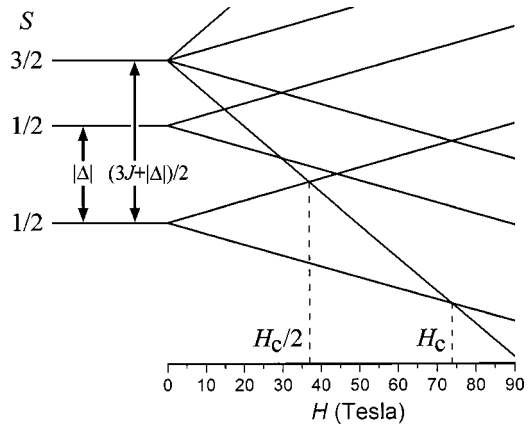

FIG. 2. Energy levels vs magnetic field H for the Heisenberg Hamiltonian of Eq. (1) for the choices of J, Δ, and g adopted in Sec. II C 1. Note that for $H<H_c\equiv(3J+|\Delta|)/(2\mu)\approx 74$ T the total spin quantum number of the ground state level is $S=1/2$, whereas for $H>H_c$ it is given by $S=3/2$.

B. Isospectrality

In our choice of the model Hamiltonian of Eq. (1) we have explicitly assumed that spin 1 interacts with spins 2 and 3 with the same exchange energy J_a. This assumption is justified for **1** by the fact that, first, the distances between spins 1, 2 and between spins 1, 3 are virtually identical (3.22 Å) and, second, by the existence of identical exchange pathways [see Fig. 1(b)]. However, for **2** the corresponding distances are 3.21 and 3.25 Å. Especially for the latter compound it is of interest to consider the possibility of three distinct exchange energies J_{12} between spins 1 and 2, J_{23} between spins 2 and 3, and finally J_{31} between spins 3 and 1. It turns out, however, that, first,[13] the resulting Hamiltonian in zero field has only three distinct energy eigenvalues and, second,[9,12] there is a continuous family of choices of J_{12}, J_{23}, and J_{31} that shares the very same three energies. These, so-called, isospectral systems can be characterized geometrically in terms of a circle in the Cartesian space defined by three orthogonal axes, one for each of the variables J_{12}, J_{23}, and J_{31}. Specifically, the continuous set of points on the circle of radius $\sqrt{2/3}\Delta$, whose center has coordinates $J_{12}=J_{23}=J_{31}=J$ and whose normal is parallel to the unit vector $(1/\sqrt{3})(\hat{i}+\hat{j}+\hat{k})$ define an isospectral family with the common three energies $-(3/4)J\pm|\Delta|/2$ and $(3/4)J$. The practical relevance of isospectrality is that, even if there are three different exchange constants in **2**, measurements of thermodynamic quantities, such as $M(T,H)$ or the magnetic specific heat, which are fixed by the values of the energy levels of the Heisenberg triangle, can only provide two parameters J and Δ. Equivalently, we can model this system using only two exchange constants, with the choices $J_{12}=J_{31}=J_a\equiv J+(\Delta/3)$ and $J_{23}=J_c\equiv J-(2\Delta/3)$.

Apart from the Heisenberg model of three spins 1/2, there are several other isospectral Heisenberg model systems that have been identified,[9] but overall the total number of such

exceptional systems is very small. Isospectral systems are of interest since they contradict the usual expectation that comparison between measured data and the corresponding prediction of the theory—say, for the temperature-dependent magnetic susceptibility—will yield unique exchange energies.

C. Thermodynamic properties

Using the above energies, it is a straightforward exercise to derive the form of the partition function of a single Heisenberg isosceles triangle,

$$Z = 4\cosh\left(\frac{\mu H}{2k_BT}\right)\left[e^{-3J/4k_BT}\cosh\left(\frac{\mu H}{k_BT}\right) + e^{3J/4k_BT}\cosh\left(\frac{\Delta}{2k_BT}\right)\right]. \tag{3}$$

Note that the partition function is left invariant when the sign of Δ is reversed. Hence a thermodynamic measurement can only yield values of J and $|\Delta|$. From the partition function one easily derives the paramagnetic contribution to the magnetic moment. With this model we arrive at the following formula for the temperature- and field-dependent molar magnetization of **1** and **2**:

$$M(T,H) = \chi_0 H + N_A\mu\left[\tanh\left(\frac{\mu H}{2k_BT}\right) + \frac{2\sinh\left(\frac{\mu H}{k_BT}\right)}{\cosh\left(\frac{\mu H}{k_BT}\right) + \exp\left(\frac{3J}{2k_BT}\right)\cosh\left(\frac{\Delta}{2k_BT}\right)}\right], \tag{4}$$

where χ_0 is the molar diamagnetic susceptibility, N_A is Avogadro's number, and k_B is Boltzmann's constant. The contribution of a single Heisenberg isosceles triangle to the specific heat follows from Eq. (3) using the standard statistical-mechanical formula

$$C = k_BT\partial^2(T\ln Z)/\partial T^2. \tag{5}$$

1. Low-field susceptibility

The physical content of Eq. (4) is easily established. Suppose first that H is held fixed and that $k_BT \ll |\Delta|/2$ as well as $\mu H \ll (3J+|\Delta|)/2$. In this temperature regime the second term within the square brackets of Eq. (4) can be ignored and we have

$$M(T, H=\text{const}) \approx \chi_0 H + N_A\mu\tanh\left(\frac{\mu H}{2k_BT}\right). \tag{6}$$

That is, in this temperature regime the paramagnetic behavior of a mole of the compound can be pictured as that of an array of $2N_A$ noninteracting triangles, each to be pictured as a single spin-1/2 particle with magnetic moment $g\mu_B/2$. As the temperature is raised and the more restrictive conditions $\mu H \ll k_BT \ll (3J+|\Delta|)/2$ apply, we may further approximate Eq. (6) to obtain

$$T\chi \approx T\chi_0 + N_A(g\mu_B)^2/(2k_B), \tag{7}$$

where $\chi = M/H$. For these low temperatures the diamagnetic term $T\chi_0$ in Eq. (7) can safely be ignored and we arrive at the prediction that $T\chi$ will saturate as the temperature is raised, while satisfying the above inequality, and a measurement of that saturated value can be used to fix the numerical value of g. In fact, this is the procedure used below. For still higher temperatures the second term of Eq. (4) begins to contribute significantly; $T\chi$ increases, and ultimately, when $k_BT \gg 3J/2, |\Delta|/2$, it saturates to

$$T\chi \approx T\chi_0 + 3N_A(g\mu_B)^2/(2k_B). \tag{8}$$

The factor of 3 in Eq. (8) reflects the fact that in this high-temperature regime the exchange interaction between each spin is ignorable; i.e., each triangle may be pictured as three independent spins 1/2 and the limiting, Curie law behavior is achieved. As seen in the following, this feature, of a factor of 3 ratio for these two saturation values of Eqs. (7) and (8), is fulfilled for our experimental data for $T\chi$.

Measurements of magnetization versus temperature were performed at 0.5 T using Quantum Design MPMS superconducting quantum interference device (SQUID) magnetometers. Shown in Fig. 3 are our experimental data for the quantity $T\chi$ for **1** for temperatures between 1.9 and 290 K. In the inset, error bars at the level of 0.5% have been attached representing measurement and mass determination uncertainties. Note that the data do in fact saturate in the range 5–12 K, as anticipated above. Using the measured saturated value of $T\chi$ (0.71 emu K/mol) along with Eq. (7), one finds that $g = 1.95$. The onset of saturation is also visible for $T > 150$ K as anticipated above with $T\chi$ approaching the theoretical prediction of 2.1 emu K/mol—i.e., a factor of 3 larger than the saturated value in the low-temperature range. We have applied a least-squares fitting routine to our data using the general formula of Eq. (4), and we find that $J = 45.3 \pm 0.2$ K, $\Delta = 57.7 \pm 1.4$ K, and the diamagnetic contribution equals $\chi_0 = -2.1 \times 10^{-4}$ emu/mol. Note the excellent agreement for all T that results in Fig. 3 upon adopting these choices of parameters. The corresponding exchange energies are thus given by $J_a = 64.6 \pm 0.5$ K and $J_c = 6.9 \pm 1$ K. For **2** we find that $g = 1.954$ and the results of least-squares fitting are $J = 44.5 \pm 0.3$ K, $\Delta = 58.0 \pm 1.6$ K, and $\chi_0 = -2.2 \times 10^{-4}$ emu/mol. Here the exchange energies are given by

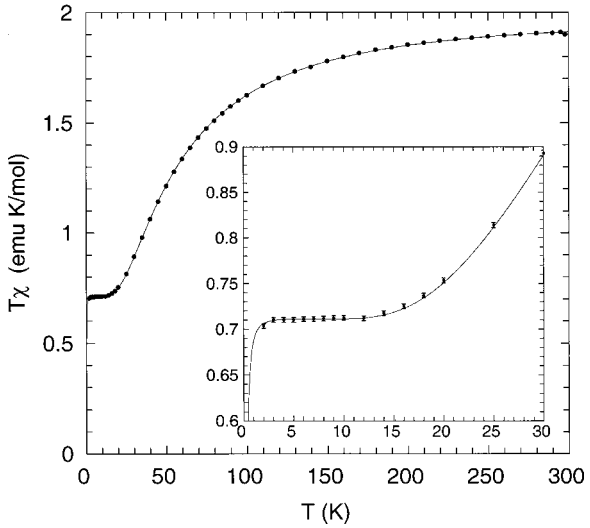

FIG. 3. $T\chi$ vs T for compound **1** for an external field $H=0.5$ T. The error bars on the experimental data shown in the inset are drawn for an estimated level of 0.5%. The solid curve is the theoretical result based on the Heisenberg Hamiltonian of Eq. (1) for the choices of J, Δ, and g made in Sec. II C 1.

$J_a=63.8\pm0.6$ K and $J_c=5.9\pm1.1$ K. The same high-quality fit has been achieved, but we have not displayed the corresponding figure as it looks nearly identical to Fig. 3.

Now that the exchange energies have been determined, the spacings of the three field-free magnetic energy levels are known and we have well-defined theoretical predictions which we compare to the results of the experimental probes that are discussed in the remainder of this paper.

2. M versus H

Returning to the general expression, Eq. (4), we suppose now that T is maintained constant and we study the Zeeman splitting of energy levels as H is increased. It is convenient to define a critical magnetic field

$$H_C \equiv (3J+|\Delta|)/(2\mu), \tag{9}$$

corresponding to the intersection of the two lowest energy levels (see Fig. 2). In particular, for $H<H_c$ the ground-state energy level has quantum numbers $S=1/2$, $M_S=-1/2$, whereas for $H>H_c$ the quantum numbers are $S=3/2$, $M_S=-3/2$. It follows that, in the low-temperature limit, the paramagnetic contribution to $M(0,H)$ saturates to the values $N_A\mu$ for $H<H_c$ and to $3N_A\mu$ for $H>H_c$. As the temperature is gradually raised from 0 K, the major features of the *M-H* curves are that the pronounced plateaus (values $N_A\mu$ and $3N_A\mu$) begin to wash out, yet at sufficiently low temperatures, to an excellent approximation the curves intersect at both $H_c/2$ and H_c, with values $N_A\mu$ and $2N_A\mu$, respectively, as seen in Fig. 4. It can be shown[14] that the common intersection at low temperatures for $H_c/2$ is associated with the intersection of the excited $S=1/2$, $M_S=1/2$ and $S=3/2$, $M_S=-3/2$ energy levels (see Fig. 2). The common intersections of the *M-H* curves at $H_c/2$ and H_c gradually break down as the temperature is raised. Using Eq. (9), we note that the critical field is given by $H_c=73.9\pm0.7$ for **1** and 73.0 ± 0.9 for **2**.

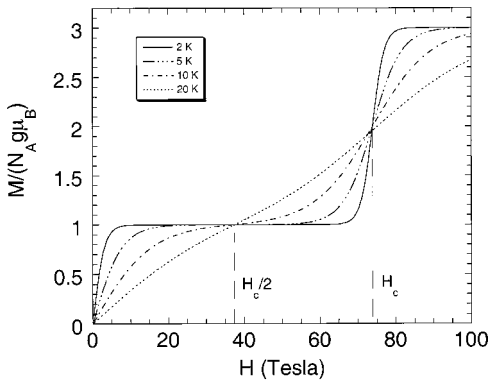

FIG. 4. Magnetization vs magnetic field H for the Heisenberg model of Eq. (1) and choices of parameters adopted in Sec. II C 1.

In the following we provide our experimental results for M versus H for several low temperatures as obtained, first, using a static field extending to 18 T and, second, using a pulsed field extending to 60 T. Both sets of measurements were obtained using facilities at the National High Magnetic Field Laboratory, Los Alamos, NM. These results are compared with the theoretical formulas derived for the Heisenberg triangles using the values of J_a, J_c, and g found in Sec. II C 1.

In Fig. 5 we display our experimental results for M as obtained for **1** using static fields for $T=2.0$, 3.0, 4.0, and 10.0 K. The measurements were obtained with a vibrating sample magnetometer (PAR model 4500) operating in the longitudinal field of a 20 T superconducting magnet. The sample was located in the He-gas stream of a variable temperature insert. The temperature of the heat exchanger was stabilized with a temperature controller and we used Cernox* thin film resistance temperature sensors. For this range of temperatures and for fields extending up to 18 T, the

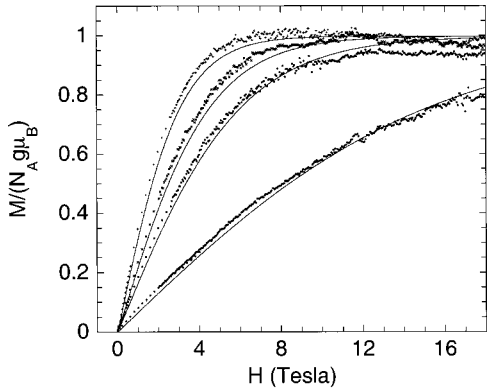

FIG. 5. Comparison between experiment and theory (including diamagnetic contribution) for the magnetization M of compound **1** for static magnetic fields H up to 18 T for $T=2,3,4,10$ K. As discussed in the text, for the choices of J, Δ, and g made in Sec. II C 1, the paramagnetic behavior in this regime of temperatures and fields is accurately described in terms of noninteracting triangles each pictured as a single spin-1/2 particle.

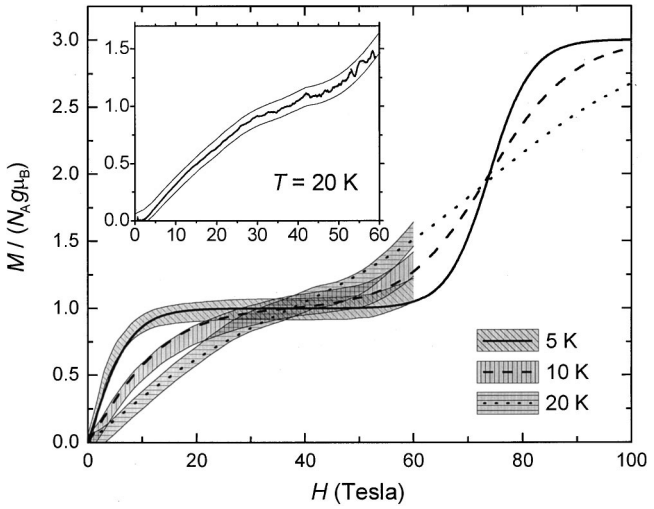

FIG. 6. Experimental determination of the magnetization of compound **1** as a function of magnetic field, up to 60 T, as obtained using a pulsed-field technique. Isothermal measurements were performed at 5, 10, and 20 K. The inset shows a typical measurement curve (for 20 K) together with the estimated maximum systematic error boundary curves of the experiment. In the main figure we present only the error boundary curves (shown as shaded hatched areas) as well as the theoretical (solid, dashed, and dotted) curves for these temperatures.

simplified formula of Eq. (6) can be used for constructing the corresponding theoretical curves. As remarked in Sec. II C 1, for this regime the paramagnetic behavior can be pictured as that of an array of noninteracting triangles with each to be pictured as a single spin-1/2 particle. The theoretical curves including the diamagnetic contribution are shown as the continuous curves in Fig. 5. Theory and experiment are in very good agreement.

High-field magnetization experiments were performed in a 60-T pulsed-field solenoid with a 20-ms nominal pulse length. The magnetization was measured using a compensated set of pickup coils. Utilizing fast digitizers, the inductive method provides data for dM/dt and dH/dt, which are subsequently integrated to give results for M versus H. After background subtraction the measured data have been normalized to our absolute low-field (SQUID) results for each choice of temperature. Because of the absence of eddy currents within the electrically insulating sample, the temperature during the 20-ms field pulse stayed within 10% of the controlled ambient temperature. Shown in Fig. 6 are the results of measurements at temperatures 5, 10, and 20 K. The bounding error curves shown in the main portion of Fig. 6 represent conservative choices of statistical as well as systematic errors based on the reproducibility of the experiment. The corresponding theoretical results derived using the general formula of Eq. (4) are shown as the solid, dashed, and dotted curves. The experimental data are consistent with our theoretical prediction (Sec. II A) that for these temperatures the curves should intersect at $H_c/2 \approx 37$ T, although in view of the large spread in the experimental error bounding curves we can only estimate that $(H_c/2)_{\text{expt}} = 40 \pm 10$ T. Clearly, it would be desirable to reexamine this feature in future studies. In any event, the experiment does confirm the prediction of theory that for low fields the *M-H* curves are sequenced such that the higher curve is associated with the lower temperature, while for large fields the reverse order applies. In the range 50–60 T the rapid rise of the experimental data might be suggestive of a somewhat lower value of the critical field than the theoretical prediction. However, in view of the very large spread in the error bounding curves we do not cite this as a definitive result.

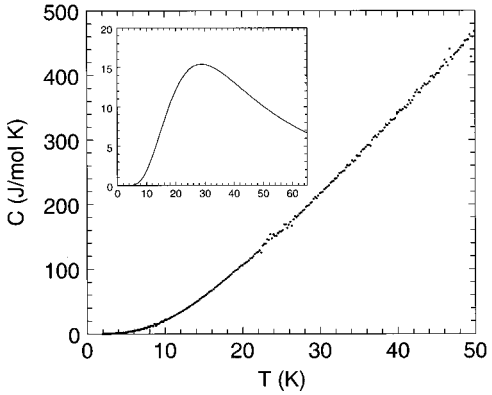

FIG. 7. Experimental molar specific heat vs temperature for $H = 0$. In the inset we give the theoretical paramagnetic contribution.

3. Specific heat

The contribution of the interacting spin system to the specific heat is another thermodynamic quantity of interest. This quantity is easily calculated using Eqs. (3) and (5), and the results for $H = 0$ are shown in the inset of Fig. 7 using the values of J and Δ derived for **1**. The overall behavior is very similar to that of a standard Schottky peak associated with a two-level magnetic system. However, the spin triangle has three energy levels and this gives rise to some modifications. Note the broad maximum with a peak value of about 15 J/(mol K) at 28.5 K and a very slow decrease to zero, which is proportional to $1/T^2$ at high temperatures. Direct observation of the spin contribution to the specific heat is rather difficult since, as discussed below, the background lattice contribution grows very rapidly with increasing temperature and virtually masks the spin contribution.

We have measured the specific heat of **1** over the temperature range from 2 to 50 K for both $H = 0$ and 9 T using the heat capacity option of a Quantum Design PPMS instrument. The results for $H = 0$ are shown in Fig. 7. The measured specific heat at the peak temperature, 28.5 K, of the spin contribution is approximately 200 J/(mol K), and rising very rapidly as a result of the background lattice contribution. It was therefore not possible to identify the superimposed paramagnetic contribution. Also the unavailability of a nonmagnetic analog precluded any attempt to extract the paramagnetic contribution by a subtraction procedure, for example, subtracting the zero-field results of the magnetic and nonmagnetic analogs. While the temperature dependence of the measured specific heat could not be accurately reproduced using the Debye theory, we estimate that the Debye temperature is 190 ± 20 K.

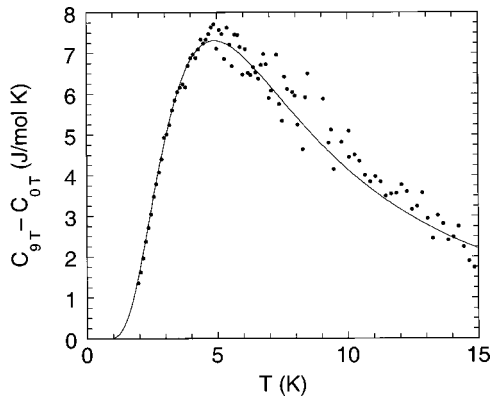

FIG. 8. Experimental (solid circles) and theoretical (solid curve) results for the specific heat difference $C(T,H)-C(T,0)$ vs T for a magnetic field $H=9$ T.

For the experimentally accessible regime of field values (up to 9 T) the values of H are quite small compared to the critical field H_c. One can therefore totally ignore the field-dependent term in the right most factor of the partition function of Eq. (3). That is, the paramagnetic specific heat *difference* can be derived exclusively from the first factor of Eq. (3) or, equivalently, from the expression $F=-k_BT\ln[\cosh(\mu H/2k_BT)]$ for the free energy of a spin triangle treated as an independent spin-1/2 particle in an external magnetic field. Note in particular that the values of the exchange parameters J and Δ do not enter into this theoretical expression. In this manner one arrives at the approximate formula for the field-induced deviation in the molar specific heat difference:

$$C(T,H)-C(T,0)=2N_Ak_B\left(\frac{\mu H}{k_BT}\right)^2\operatorname{sech}^2\left(\frac{\mu H}{k_BT}\right). \quad (10)$$

This theoretical result is shown as the solid curve in Fig. 8.

The experimental specific heat difference $C(T,H)-C(T,0)$, for $H=9$ T, can be expected to given by the simple theoretical formula of Eq. (10) if one makes the reasonable assumption that the lattice contribution to the measured specific heat is independent of H. Indeed our data for **1**, shown in Fig. 8, are in very good agreement with the theoretical expression of Eq. (10). This provides direct confirmation of the fact that in this field range the compound behaves as a collection of independent spin triangles each to be pictured as a spin-1/2 entity.

III. SPIN-LATTICE RELAXATION RATES

A. Experimental background

The measurement of the nuclear spin-lattice relaxation rate (NSLR) $1/T_1$ using NMR techniques provides an effective technique for determining the low-frequency characteristics of the dynamics of the paramagnetic ions in magnetic molecules. In essence, the results for $1/T_1$ are used to probe the fluctuation spectrum of the paramagnetic moments, which are coupled via dipole-dipole interactions to hydrogen or other selective nuclei.

We have performed extensive measurements of $1/T_1$ both for ^{1}H and ^{23}Na nuclei for polycrystalline samples of both **1** and **2** in the temperature range 1.5–300 K. Of particular interest are the results using ^{23}Na nuclei since their small number per magnetic molecule provides a more discriminating reading of the dynamics of the V^{4+} spins. For example, in the case of **1** the measurement of $1/T_1$ provides the reading by a single Na nucleus of the dynamics of its adjacent Heisenberg triangle of V spins. The proton NMR data constitute an average reading for a large number of ^{1}H nuclei with inequivalent spatial locations.

Measurements were made using a phase-coherent spin-echo spectrometer. The NMR spectrum was determined from the Fourier transform of the half-echo signal obtained by using the typical two-pulse Hahn echo. The $\pi/2$ pulse lengths were 2–4 and 3–5 μs for ^{1}H and ^{23}Na, respectively, depending on the operating frequency of the spectrometer. In all cases the strength of the rf field H_1 was sufficient to irradiate the whole NMR line. The value of $1/T_1$ was obtained by monitoring the recovery of the nuclear magnetization following a short sequence of saturating rf pulses. In the case of ^{1}H NMR the recovery curve was nonexponential due to the existence of sets of nonequivalent ^{1}H sites in the molecule, each set associated with its own relaxation rate. We followed the common practice[15] of determining $1/T_1$ by measuring the initial slope of the recovery curve since this quantity provides a weighted average of the nonequivalent sites of the probe nuclei in the magnetic molecule.

In the case of ^{23}Na ($I=3/2$), only the central transition was irradiated because of the presence of sizeable quadrupole effects. Thus $1/T_1$ was established by using a saturation recovery pulse sequence and fitting the data to the recovery formula

$$1-M(t)/M(\infty)=0.1\exp(-t/T_1)+0.9\exp(-6t/T_1), \quad (11)$$

which is obtained from the solution of the master equation for the case of a magnetic relaxation mechanism and selective irradiation of the central transition only.[16]

B. Experimental results

The temperature dependence of $1/T_1$ obtained by ^{1}H NSLR measurements is displayed in Figs. 9(a) and 9(b) for **1** and **2**, respectively, for the fields 1.25 and 4.7 T. The field dependence of $1/T_1$ is shown in Figs. 10(a) and 10(b) for **1** and **2**, respectively, for temperatures 4.2, 24, and 294 K. In the case of **1** this body of data is well represented by the formula

$$T_1^{-1}(T,H)=\left(0.25+\frac{1.92}{H^2+1}\right)T_1^{-1}(T,1.25), \quad (12)$$

with H in tesla. In particular, according to this formula, $T_1^{-1}(T,4.7)=(1/3)T_1^{-1}(T,1.25)$, and as can be seen from Fig. 9(a), this relation is rather well satisfied. The solid

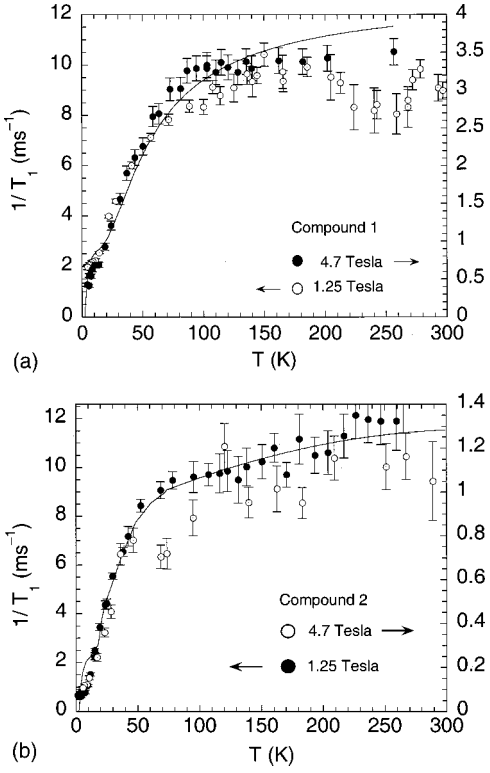

FIG. 9. Proton spin-lattice relaxation rate $1/T_1$ as a function of temperature for 1.25 and 4.7 T for compounds **1** (a) and **2** (b). Because of the factorized form of $1/T_1$ according to Eq. (12), the results in (a) for 1.25 T should be a factor of 3 larger than those for 4.7 T irrespective of the temperature. In (b), using Eq. (13), the corresponding factor should be 9. The spacings chosen for the right and left ordinate axes are consistent with these factors. The solid curves give the theoretical results obtained using Eqs. (17) and (18).

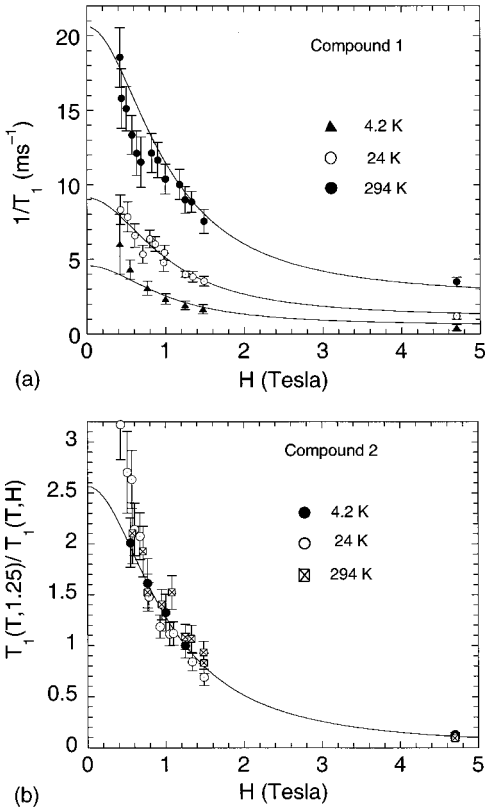

FIG. 10. Proton spin-lattice relaxation rate $1/T_1$ as a function of magnetic field for 4.2, 24, and 294 K for compounds **1** (a) and **2** (b). The solid curves in (a) satisfy Eq. (12), and those in (b) satisfy Eq. (13).

curves shown in Fig. 10(a) have been drawn using Eq. (12), and here too the fitting formula provides an accurate representation of the data.

For **2** the corresponding formula is

$$T_1^{-1}(T,H)=\frac{2.56}{H^2+1}T_1^{-1}(T,1.25). \tag{13}$$

In particular, for this compound we have $T_1^{-1}(T,4.7) \approx (1/9)T_1^{-1}(T,1.25)$. Inspection of Fig. 9(b) shows that this relation is consistent with our experimental data. In Fig. 10(b) we have plotted the values of $T_1(T,1.25)/T_1(T,H)$ versus H for the three temperatures 4.2, 24, and 294 K. According to Eq. (13), the data points should lie on the (solid) curve $2.56/(H^2+1)$. This is fulfilled except for the three data points for the smallest measured values of H at 24 K.

The formulas of Eqs. (12) and (13) imply the separability of T_1^{-1} into a product of two factors, one of which is temperature dependent and the other field dependent. The practical importance of this property lies in the fact that knowledge of the temperature dependence of T_1^{-1} for one value of H provides the temperature dependence for any other value of H. A plausible theoretical explanation for this separability is given in the following subsection. We also give a sketch of our first-principles derivation of the temperature dependence of T_1^{-1}.

We note that the temperature dependence of the spin-lattice relaxation rate is not adequately described by the common phenomenological formula[11] giving $1/T_1$ proportional to $T\chi(T)$. The simplest way to confirm this statement is to note that the property derived in Sec. II C1—namely, that there is

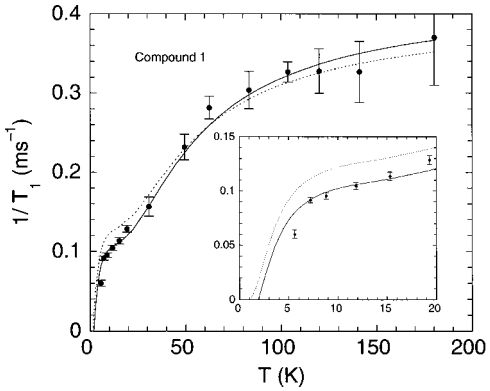

FIG. 11. ^{23}Na spin-lattice relaxation rate $1/T_1$ as a function of temperature for 4.7 T for compound **1**. The solid curve satisfies Eq. (17), while the dashed curve is proportional to $T\chi(T)$. The results for temperatures below 20 K are displayed in the inset.

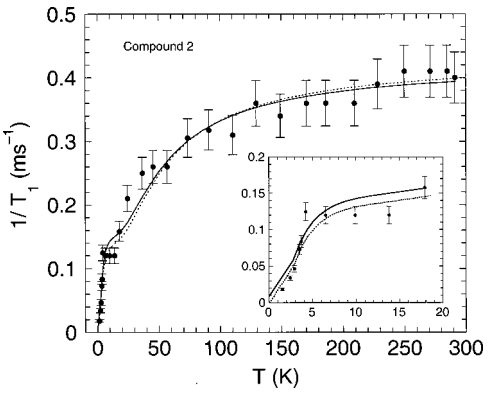

FIG. 12. ^{23}Na spin-lattice relaxation rate $1/T_1$ as a function of temperature for 4.7 T for compound **2**. The solid curve satisfies Eq. (17), while the dashed curve is proportional to $T\chi(T)$. The results for temperatures below 20 K are displayed in the inset.

a 3:1 ratio between the saturation values associated with the two plateaus of $T\chi(T)$—is not fulfilled by the spin-lattice relaxation data.

In Figs. 11 and 12 we present our data for the temperature dependence of $1/T_1$ obtained by ^{23}Na NSLR measurements in **1** and **2** in a field of 4.7 T. Qualitatively, the temperature dependence appears to be similar to that of the ^{1}H NSLR measurements shown in Figs. 9(a) and 9(b); however, the theoretical discussion in the following subsection will highlight the differences.

C. Theoretical discussion

To explain our experimental results of the previous subsection we have calculated the two-spin time correlation functions appropriate for the paramagnetic ions. According to the standard formula of Moriya,[10] which is based on a first-principles perturbative treatment of the hyperfine interactions between nuclear and paramagnetic spins, $1/T_1$ is given by a linear combination of Fourier integrals,

$$\tilde{C}^{jk}_{\alpha\alpha}(\omega_N,T,H)\equiv\int_0^\infty dt C^{jk}_{\alpha\alpha}(t,T,H)\cos(\omega_N t), \qquad (14)$$

of the equilibrium time correlation functions

$$C^{jk}_{\alpha\alpha}(t,T,H)\equiv\langle\delta S_{j\alpha}(t)\,\delta S_{k\alpha}(0)\rangle \qquad (15)$$

for the $\alpha\,(=x,y,z)$ component of the spin operators associated with the pair of spins j and k. Here $\langle\cdots\rangle=(1/Z)\mathrm{Tr}(e^{-\beta\mathcal{H}}(\cdots))$ denotes the canonical ensemble average based on the Hamiltonian $\mathcal{H}$ of Eq. (1) and the operator $\delta S_{i\alpha}(t)$ is defined by $\delta S_{i\alpha}(t)\equiv\exp(i\mathcal{H}t/\hbar)S_{i\alpha}\times\exp(-i\mathcal{H}t/\hbar)-\langle S_{i\alpha}\rangle$. The integral in Eq. (14) is evaluated at the nuclear Larmor angular frequency $\omega_N(\mathrm{MHz})=267.5H$, associated with the given measuring magnetic field (in tesla). The coefficients of the linear combination of integrals, Eq. (14), providing $1/T_1$ are the (temperature-independent) components of the magnetic dipole interaction tensor.[10] Neglecting second-order effects of H, we have

$$C^{jk}_{xx}(t,T,H)=C^{jk}_{yy}(t,T,H)\approx C^{jk}_{zz}(t,T,0)\cos(\omega_e t) \qquad (16)$$

and $C^{jk}_{zz}(t,T,H)\approx C^{jk}_{zz}(t,T,0)$. Here $\omega_e(\mathrm{GHz})=176H$ denotes the electron Larmor angular frequency.

The evaluation of $C^{jk}_{zz}(t,T,H)$ within our model of the isosceles Heisenberg triangle shows that this function consists of several terms whose time dependence is of the form $\exp(\pm i\Omega t)$, where Ω takes on four values, $\Omega=0$, and the three angular frequencies Ω_{ex} associated with transitions between the two $S=1/2$ and $S=3/2$ energy levels. The Fourier integral $\tilde{C}^{jk}_{zz}(\omega_N,T,H)$ therefore reduces to a sum of terms which we write as $f^{jk}(T,\Omega)\,\delta(\omega_N-\Omega)$, one for each of the above choices of Ω. Using Eq. (16), it follows that the Fourier integrals $\tilde{C}^{jk}_{xx}(\omega_N,T,H)$ and $\tilde{C}^{jk}_{yy}(\omega_N,T,H)$ are sums of terms of the form $f^{jk}(T)\,\delta(\omega_N-\Omega\pm\omega_e)$. However, given that $\omega_N,\ \omega_e\ll\Omega_{\mathrm{ex}}$, the only terms which might realistically contribute to $1/T_1$ are $f^{jk}(T)\,\delta(\omega_N)$ and $f^{jk}(T)\,\delta(\omega_e\pm\omega_N)$. This corresponds to the fact that only quasistatic fluctuations allow for energy-conserving nuclear transitions at ω_N, $\omega_e\pm\omega_N$. In actual fact we expect that these δ functions are somewhat broadened to Lorentzians in the real material. Thus we obtain the following expression for the temperature and field dependence of $1/T_1$:

$$T_1^{-1}(T,H)=F_{zz}(T)[\,\omega_0/(\omega_N^2+\omega_0^2)+\alpha\omega_0/(\omega_e^2+\omega_0^2)], \qquad (17)$$

where ω_0 is an angular frequency measuring the Lorentz broadening, α is a constant which measures the ratio between components of the magnetic dipole interaction tensor, and

$$F_{zz}(T)=a[f^{11}(T)+2\,f^{22}(T)]+b[2\,f^{12}(T)+f^{23}(T)]. \qquad (18)$$

The constants a and b can be expressed in terms the magnetic dipole interaction tensor elements. In particular, the detailed temperature dependence of $1/T_1$ is set by that of the nonequivalent autocorrelation (f^{11} and f^{22}) and nearest-neighbor (f^{12} and f^{23}) correlation functions. Note the separability of Eq. (17) into a product of temperature- and field-dependent factors as well as the overall similarity to the expressions of Eqs. (12) and (13), which summarize our experimental findings for proton NMR. The similarity is closer yet when $\omega_0\gg\omega_N$, for then we can approximate Eq. (17) by

$$T_1^{-1}(T,H)=F_{zz}(T)[\,1/\omega_0+\alpha\omega_0/(\omega_e^2+\omega_0^2)], \qquad (17')$$

which is consistent with Eq. (12). Moreover, if $\alpha\gg1$, we may use the simplified relation

$$T_1^{-1}(T,H)=F_{zz}(T)\,\alpha\omega_0/(\omega_e^2+\omega_0^2), \qquad (17'')$$

which is consistent with Eq. (13).

Comparing Eqs. (17′) and (17″) to Eqs. (12) and (13) we conclude that, for both **1** and **2**, $\omega_0\approx1.8\times10^{11}$ Hz. Because of the very similar structure of these two compounds, it is not at all surprising that the value of the broadening parameter is the same. Results of the same order of magnitude have

been reported[17] for other magnetic molecules. In the following section we attribute this value of ω_0 to a weak intertriangle exchange interaction of approximate strength 0.3 K.

We typically determined a and b by a least-squares fit to the proton and ^{23}Na data obtained for a magnetic field of 4.7 T. The one exception was that we used proton data taken at 1.25 T for **2** as the error bars are distinctly smaller than for the 4.7 T data. In the case of the proton data we find $a=4.94$, $b=13.45$ and $a=1.45$, $b=3.97$ for **1** and **2**, respectively. Using these values of a and b along with Eqs. (17) and (18), we obtain the solid curves shown in Figs. 9(a) and 9(b). We also note that if one uses the standard susceptibility-fluctuation formula, one can show that if $2a/b=1$, the right-hand side of Eq. (18) is then proportional to $T\chi(T)$. Instead, for both **1** and **2** we have $2a/b\approx 0.73$. This explains the fact, noted in the previous subsection, that the measured temperature dependence of $1/T_1$ is not adequately described by the phenomenological, approximate formula proportional to $T\chi(T)$. That the same value of $2a/b$ describes both compounds is probably due to the very similar geometrical arrangement of the vanadium ions in the two compounds and especially the fact that there is a very large number of H nuclei, essentially uniformly distributed about each vanadium triangle.

For the ^{23}Na data the results are $a=0.525$, $b=1.252$ and $a=0.6$, $b=1.09$ for **1** and **2**, respectively. The resulting theoretical curves for $1/T_1$ are displayed (solid curve) in Figs. 11 and 12 together with that obtained based on the common phenomenological formula[11] giving $1/T_1$, proportional to $T\chi(T)$ (dashed curve). The close agreement between the solid and dashed theoretical curves is due to the fact that the least-squares results for a and b nearly fulfill the relation $2a/b=1$.

IV. DISCUSSION AND SUMMARY

In this work we have presented comprehensive experimental and theoretical results that are generally in very good agreement for two species of magnetic molecules of the type $\{V_6\}$. The theoretical results were obtained from exact calculations based on the isotropic Heisenberg Hamiltonian for a triangular array of exchange-coupled spin-1/2 VO^{2+} ions. The antiferromagnetic exchange interaction between two pairs of ions was found to be an order of magnitude larger than that of the third pair, even though the distances between the ions differ by only 5%. We attribute the great disparity in the exchange constants to the absence of an O-P-O exchange pathway[8] linking the third pair of VO^{2+} ions. The excellent agreement between theory and experiment for $T\chi$ for all temperatures measured (>2 K) indicates that the intertriangle exchange interaction[18] is less than 0.3 K, some two orders of magnitude smaller than the strongest intratriangle exchange constant J_a. Besides the relatively large intertriangle V-V distances (>4.6 Å), we attribute the weak intertriangle exchange interaction to the different geometric parameters of the V-O-P-O-V links, with the V-O-P bond angles displaying the most pronounced differences (intratriangle, 126.4°–128.9°; intertriangle, 136.4°–137.0°). In addition, all five atomic positions of the intratriangle V-O-P-O-V groups approximately lie within a plane, which is not the case for the corresponding intertriangle V-O-P-O-V groups. Further support for our claim of a very weak intertriangle exchange interaction is provided by the proton NMR spin-lattice relaxation data. An important parameter derived from the fit of that data is the level broadening parameter $\omega_0 \approx 1.8\times 10^{11}$ Hz for both **1** and **2**. This value was derived using the fact that the field-dependent Lorentzian factor in Eqs. (12) and (13) has a width parameter of 1 T. That ω_0 is temperature independent would appear to rule out a dominant contribution from spin-phonon lifetime effects. A temperature-independent broadening of this magnitude could arise from an intertriangle exchange interaction[18] $J_{\text{inter}} \approx 0.3$ K, if we identify ω_0 with the exchange frequency[10] $\omega_x = \frac{8}{3} zS(S+1)(J_{\text{inter}})^2/\hbar^2 = 1.6\times 10^{11}$ Hz, where $z=2$ is the number of exchange-coupled triangles and $S=1/2$.

If an underlying Heisenberg triangular unit is subject to an external magnetic field H which is smaller than a critical value H_c, the total spin quantum number of the ground state is $S=1/2$, whereas if H exceeds H_c, one has $S=3/2$. A theoretical expression for H_c, Eq. (9), was derived in Sec. II A1. The physical origin of this transition is that below H_c the antiferromagnetic coupling between spins is sufficiently strong to maintain a spin-compensated ground state, as the quantum analog of a frustrated classical ground state for three spins. Above H_c, the external magnetic field is sufficiently strong to overcome the antiferromagnetic exchange and to align the three spins parallel. One can also picture this phenomenon in terms of the crossing of the two lowest-energy levels when H exceeds H_c. The idealized signature of this phenomenon is that at absolute zero the magnetization is field independent up to H_c and suddenly increases by a factor of 3 and remains field independent for larger values of H. For the two species of magnetic molecules studied in this work the predicted values of H_c are approximately 74 T. Increasing the temperature from absolute zero, the sharp features of this picture of M versus H in terms of two plateaus are progressively washed out, approaching the standard linear behavior. Nevertheless, the theoretical prediction is that for temperatures below 10 K, the modifications in the first plateau are modest and additionally the magnetization curves for different temperatures intersect at $H_c/2$ (see Fig. 4). Within the limitations of the rather large experimental error of the pulsed-field measurements, the data shown in Fig. 6 are consistent with these theoretical results, although the field-induced spin transition could not be directly observed. Finally, the theoretical results for the spin-lattice relaxation time, obtained by calculation of the equilibrium time correlation functions, are in good agreement with the measured ^{1}H and ^{23}Na spin-lattice relaxation rates.

The energy levels of the Heisenberg Hamiltonian, their associated quantum numbers, and their dependence on magnetic field are shown in Fig. 2. In particular note that the lowest two ($S=1/2$) levels would be degenerate if $J_a=J_c$. Using the numerical values of the exchange constants, the predicted energies of the first excited level ($S=1/2$) and the second excited level ($S=3/2$), measured from the ground-state level ($S=1/2$), are 5.0 and 8.25 meV, respectively. Indeed, definitive peaks have been observed in the neutron

absorption spectrum of a deuterated derivative of **2** at essentially these energies, thereby providing independent confirmation of our exchange constant assignments. Those results will be reported elsewhere.[19]

ACKNOWLEDGMENTS

Ames Laboratory is operated for the U.S. Department of Energy by Iowa State University under Contract No. W-7405-Eng-82. One of the authors (B.J.S.) acknowledges support by KOSEF via the Electron Spin Science Center at POSTECH. We thank the National Science Foundation and the Deutscher Akademischer Austauschdienst for supporting a mutual exchange program. We acknowledge the significant assistance of N. Harrison and A. Lacerda (NHMFL-LANL) and Z. H. Jang. We also thank D. C. Johnston for useful discussions.

APPENDIX: CHEMICAL STRUCTURE DETAILS

The $[H_4V_6^{IV}O_8(PO_4)_4\{(OCH_2)_3CCH_2OH\}_2]^{6-}$ anion, abbreviated as $\{V_6\}$, can be crystallized out of an aqueous reaction solution as a green sodium-guadinium salt **1** or a blue sodium salt **2**. $(\underline{C}N_3H_6)_4Na_2\{V_6\}\cdot 14H_2O$ **1** crystallizes in the space group $P\bar{1}$ [$a=10.908(1)$ Å, $b=12.400(2)$ Å, $c=12.547(6)$ Å; $\alpha=65.695°$, $\beta=84.622°$, $\gamma=65.511°$], each unit cell hosting one $\{V_6\}$ anion. As the crystallographic inversion center defines the midpoint of the $\{V_6\}$ cluster, the cluster anion consists of two symmetry-identical halves. In each part, three vanadyl ($V=O^{2+}$) groups are coordinated (1) to a μ_3-OH ligand *trans*-positioned to the V=O groups and (2) to a pentaerythritol $(OCH_2)_3CCH_2OH$ tripod ligand via three μ_3-O positions, thereby forcing a triangular V_3 arrangement. To complete the anion structure, the two V_3 triangles are interlinked by four phosphate ligands where one O center of the phosphate binds to a V center of one V_3 ring and two O centers bind to two V centers of the other V_3 ring (Fig. 1).

The V_3 substructure can be approximated as an isosceles triangle with two short (3.218 and 3.222 Å) and one longer (3.364 Å) V···V distance. (The values are determined to an accuracy of approximately 0.001 Å). This difference mainly stems from different coordination by the phosphate ligands. While the V centers of the shorter V···V pairs are each bridged by one phosphate ligand, the two remaining phosphate ligands bind individually to the V centers of the long V···V pair only via a single $O(PO_3)$ position, leaving the two V centers unbridged. In terms of magnetic superexchange, the longer V···V pair [the pair 2,3 in Fig. 1(a)] lacks the V-O-P(O_2)-O-V exchange path that is present for the shorter V···V pairs (1,2 and 1,3). The closest intertriangle V···V contacts in the $\{V_6\}$ cluster equal approximately 4.6 Å and magnetic intertriangle coupling should be considerably weaker. See also Sec. IV and Ref. 8.

A second $\{V_6\}$ anion, structurally virtually identical to the first anion, can also be isolated in the sodium salt $Na_6\{V_6\}\cdot 18H_2O$ **2** (space group $C2/c$; $a=26.907$ Å, $b=11.167$ Å, $c=17.039$ Å; $\alpha=\gamma=90.00°$, $\beta=98.38°$; as in **1**, the cluster is centrosymmetric). In both **1** and **2** the shortest intermolecular V···V distances are approximately 7.0 Å. In **2** the three V···V distances are 3.212, 3.253, and 3.322 Å. While the two sodium cations in **1** are situated in front of the longer V···V pair, the six Na^+ cations in **2** are surrounding the whole cluster, thereby effectively screening all vanadium positions [Fig. 1(b)].

*Corresponding author. Electronic address: luban@ameslab.gov

[1] O. Kahn, *Molecular Magnetism* (VCH, Weinheim, 1993).

[2] D. Gatteschi, Adv. Mater. **6**, 635 (1994).

[3] A. Müller, F. Peters, M. T. Pope, and D. Gatteschi, Chem. Rev. **98**, 239 (1998).

[4] Tetrahedron **20**, (2001) (issues 11–14, pp. 1115–1784) is devoted to the subject of molecular magnetism.

[5] A. Müller, S. Sarkar, S. Q. N. Shah, H. Bögge, M. Schmidtmann, Sh. Sarkar, P. Kögerler, B. Hauptfleisch, A. X. Trautwein, and V. Schünemann, Angew. Chem. Int. Ed. Engl. **38**, 3238 (1999); A. Müller, M. Luban, C. Schröder, R. Modler, P. Kögerler, M. Axenovich, J. Schnack, P. Canfield, S. Bud'ko, and N. Harrison, ChemPhysChem **2**, 517 (2001).

[6] A first study of these two species has been given in A. Müller, J. Meyer, H. Bögge, A. Stammler, and A. Botar, Chem.-Eur. J. **4**, 1388 (1998).

[7] The VO^{2+} ion is known to display spin-only $s=1/2$ paramagnetism and isotropic g values close to 2.0. See, e.g., R. L. Carlin, *Magnetochemistry* (Springer-Verlag, Berlin, 1986), p. 62.

[8] For two-leg ladder-type VOPO-type systems it has been established that the V-O-P-O-V superexchange pathway can be considerably stronger than V-O-V pathways. See, e.g., D. C. Johnston, T. Saito, and M. Azuma, Phys. Rev. B **64**, 134403 (2001).

[9] H-J. Schmidt and M. Luban, J. Phys. A **34**, 2839 (2001).

[10] T. Moriya, Prog. Theor. Phys. **16**, 23 (1956), Appendix; **28**, 371 (1962).

[11] F. Borsa and A. Rigamonti, *Magnetic Resonance of Phase Transitions* (Academic, New York, 1979), p. 79.

[12] The explicit forms of the eigenvectors of the Hamiltonian operator of Eq. (1) have been given by S. Jun (M.Sc. thesis, Iowa State University, 1999) and D. Mentrup (Diplom thesis, University of Osnabrück, 1999, http://obelix.physik.uni-osnabrueck.de/~dmentrup/).

[13] One can show that there are three distinct energy eigenvalues for the general Heisenberg Hamiltonian $\mathcal{H}=J_{12}\mathbf{S}_1\cdot\mathbf{S}_2+J_{23}\mathbf{S}_2\cdot\mathbf{S}_3+J_{31}\mathbf{S}_3\cdot\mathbf{S}_1$ for three spins 1/2 in zero field. Defining the quantity $J=(1/3)(J_{12}+J_{23}+J_{31})$, these energies are given by $(3/4)J$ and $-(3/4)J\pm(1/2)(J_{12}^2+J_{23}^2+J_{31}^2-J_{12}J_{31}-J_{23}J_{12}-J_{31}J_{23})^{1/2}$. See L. D. Landau and E. M. Lifshitz, *Quantum Mechanics (Non-Relativistic Theory)*, 3rd ed. (Butterworth/Heinemann, Oxford, 1997), Sec. 62, pp. 233–234.

[14] While the common intersection of the *M-H* curves for low temperatures at $H_c/2$ can be verified by an analysis of Eq. (4), a far simpler calculation consists of calculating the partition function and, from it, the magnetization when one ignores all but the four lowest-energy levels shown in Fig. 2. This approximate calculation leads to the conclusion that the intersection of the *M-H*

curves at $H_c/2$ occurs for all temperatures.

[15] See, for example, A. Lascialfari, D. Gatteschi, F. Borsa, and A. Cornia, Phys. Rev. B **55**, 14 341 (1997).

[16] E. R. Andrew and D. P. Tunstall, Proc. Phys. Soc. London **78**, 1 (1961).

[17] A. Lascialfari, Z. H. Jang, F. Borsa, D. Gatteschi, and A. Cornia, J. Appl. Phys. **83**, 6946 (1998).

[18] Our calculations show that if the intertriangle exchange interaction were larger than 0.3 K, this would give rise to a measurable deviation in the $T\chi$ plot below 6 K.

[19] S. E. Nagler, J. Zarestky, C. Stassis, P. Kögerler, M. Luban, and A. Müller (unpublished).